Influence of jets and decays of resonances on the triangular flow in ultrarelativistic heavy-ion collisions

J. Crkovská,[1,2] J. Bielčík,[1] L. Bravina,[3,4,5] B. H. Brusheim Johansson,[3,4] E. Zabrodin,[3,4,5,6] G. Eyyubova,[6] V. L. Korotkikh,[6] I. P. Lokhtin,[6] L. V. Malinina,[6,7] S. V. Petrushanko,[6] and A. M. Snigirev[6]

[1]*Faculty of Nuclear Sciences and Physical Engineering, Czech Technical University in Prague, CR-11519 Prague, Czech Republic*
[2]*Institut de Physique Nucléaire, CNRS-IN2P3, Université Paris-Sud, Université Paris-Saclay, F-91406 Orsay Cedex, France*
[3]*Department of Physics, University of Oslo, Postboks 1048 Blindern, N-0316 Oslo, Norway*
[4]*Frankfurt Institute for Advanced Studies, Ruth-Moufang-Straße 1, D-60438 Frankfurt am Main, Germany*
[5]*National Research Nuclear University "MEPhI" (Moscow Engineering Physics Institute), RU-115409 Moscow, Russia*
[6]*Skobeltsyn Institute of Nuclear Physics, Moscow State University, RU-119991 Moscow, Russia*
[7]*Joint Institute for Nuclear Researches, RU-141980 Dubna, Russia*

(Received 31 March 2016; revised manuscript received 19 August 2016; published 23 January 2017)

Triangular flow v_3 of identified and inclusive particles in Pb + Pb collisions at $\sqrt{s_{NN}} = 2.76$ TeV is studied as a function of centrality and transverse momentum within the HYDJET++ model. The model enables one to investigate the influence of both hard processes and final-state interactions on the harmonics of particle anisotropic flow. Decays of resonances are found to increase the magnitude of the $v_3(p_T)$ distributions at $p_T \geqslant 2$ GeV/c and shift their maxima to higher transverse momenta. The p_T-integrated triangular flow, however, becomes slightly weakened for all centralities studied. The resonance decays also modify the spectra towards the number-of-constituent-quark scaling fulfillment for the triangular flow, whereas jets are the main source of the scaling violation at the energies available at the CERN Large Hadron Collider (LHC). Comparison with the corresponding spectra of elliptic flow reveals that resonance decays and jets act in a similar manner on both $v_3(p_T)$ and $v_2(p_T)$ behavior. Obtained results are also confronted with the experimental data on differential triangular flow of identified hadrons, ratio $v_3^{1/3}(p_T)/v_2^{1/2}(p_T)$, and p_T-integrated triangular flow of charged hadrons.

DOI: 10.1103/PhysRevC.95.014910

I. INTRODUCTION

Collective flow of hadrons produced in ultrarelativistic heavy-ion collisions is one of the signals especially sensitive to the creation of even a small amount of quark-gluon plasma (QGP) [1–3]. To quantify this phenomenon an expansion of the azimuthal distribution of hadrons in a Fourier series was proposed in Refs. [4,5]:

$$\frac{dN}{d\phi} \propto 1 + 2\sum_{n=1}^{\infty} v_n \cos\left[n(\phi - \Psi_n)\right]. \tag{1}$$

Here ϕ denotes the azimuthal angle between the particle transverse momentum and the participant event plane, and Ψ_n is the azimuth of the event plane of the nth flow component. The coefficients v_n are the flow harmonics that can be found after the averaging of cosines in Eq. (1) over all particles in an event and all events in the data sample:

$$v_n = \langle\langle \cos\left[n(\phi - \Psi_n)\right]\rangle\rangle. \tag{2}$$

Modifications of the proposed analysis are possible [6], but we keep the traditional scheme to compare our results to the experimental data. For almost 20 years experimentalists and theorists have intensively investigated mainly the two lowest-order coefficients, called directed v_1 and elliptic v_2 flow, see, e.g., Refs. [7,8] and references therein, whereas the study of triangular v_3 flow and higher harmonics started not long ago [9–12].

In collisions of similar nuclei, such as gold-gold or lead-lead, the higher-order odd-flow harmonics measured with respect to the reaction plane are expected to vanish under the assumption of a symmetric energy distribution. Experiments confirm that $v_3(\Psi_2) = 0$. However, initial-state fluctuations can lead to a nonvanishing participant triangularity [9], which is approximately linear to the triangular flow in its own participant plane Ψ_3 [13,14]. In many theoretical works devoted to the investigation of the signal in heavy-ion collisions, topics such as the response of v_3 to the initial triangularity ε_3 of the collision zone and sensitivity to initial-state fluctuations and to viscosity of hot QCD matter have been treated [9,13–15]. Our study focuses mainly on the influence of jets and decays of resonances on the formation of v_3, which to our best knowledge has not been explored extensively yet (see Refs. [16] and [17]). The event generator HYDJET++ [18] is employed for the simulation of Pb + Pb collisions at $\sqrt{s_{NN}} = 2.76$ TeV.

HYDJET++ suits very well for these purposes because the model includes the treatment of both soft and hard processes and has an extensive table of hadronic resonances, including the charmed ones, with more than 400 baryonic and mesonic states. The properties of the model and the generation of the anisotropic flow in it are discussed in Sec. II. Section III presents the results on differential and integrated triangular flow of charged hadrons produced from central to (semi)peripheral Pb + Pb collisions at $\sqrt{s_{NN}} = 2.76$ TeV. Here the partial contributions of hydrodynamic processes, jets, and decays of resonances to the formation of the final v_3 are studied. Ratios $v_3^{1/3}/v_2^{1/2}$ and fulfillment of the number-of-constituent-quark (NCQ) scaling are investigated as well. Finally, conclusions are drawn in Sec. IV.

II. GENERATION OF TRIANGULAR FLOW IN HYDJET++

The Monte Carlo event generator HYDJET++ (hydrodynamics with jets) treats a relativistic heavy-ion collision as a superposition of a soft, hydrolike state, hadronized as a result of a sudden thermal freeze-out, and a hard multiparton state, where energetic partons experience collisional and radiative energy losses in an expanding quark-gluon fluid [18]. The simulation of both states proceeds independently. In the soft sector the thermalized system of hadrons is generated on the hypersurfaces of chemical and thermal freeze-out given by the parametrized relativistic hydrodynamics with preset freeze-out conditions [19,20]. This approach is similar to the THERMINATOR model [21]. The effective thermal volume of the fireball is used to calculate the mean multiplicities of hadrons produced at the freeze-out hypersurface. The volume is generated on an event-by-event basis. It is proportional to the number of wounded nucleons at a given centrality provided by the Glauber model of multiparticle scattering. The only final-state interactions taken into account are the two- and three-body decays of resonances. The table of resonances is quite extensive and contains more than 360 meson and baryon (anti)states including the charmed ones.

The next part of HYDJET++, which describes the hard partonic interactions, employs the generator PYQUEN [22] for simulation of single hard nucleon-nucleon collisions. It starts with the PYTHIA-generated initial parton distributions and generation of the spatial vertexes of jet production, proceeds with the rescattering-by-rescattering propagation of partons through the hot and dense medium, determines the partons' mean free path as well as radiative and collisional energy loss, and, finally, hadronizes the hard partons and in-medium emitted gluons according to the Lund string model. Thus for each symmetric heavy-ion collision at a given impact parameter, the mean number of jets is a product of binary NN collisions and the integral cross section of the hard process with the certain minimum momentum transfer, $p_T^{\min}$. Partons produced in initial hard scatterings with a transverse momentum transfer lower than $p_T^{\min}$ are excluded from the hard component. Their products of hadronization are added to the thermalized component of the particle spectrum. These hadrons, however, can carry only weak anisotropic flow arising because of the well-known jet-quenching effect. Details of the model can be found in Refs. [18–20,23]. It is worth noting that the combination of parametrized hydrodynamics with jets was able to explain the falloff of the elliptic flow, v_2, at high transverse momenta and violation of the mass ordering of $v_2(p_T)$ distributions for mesons and baryons at $p_T \approx 2$ GeV/c [24], to predict the violation of the number-of-constituent-quark scaling for v_2 at the energies available at the LHC [24,25], and to describe the rise of the high-p_T tail of the v_4/v_2^2 ratio at the energies available at the BNL Relativistic Heavy Ion Collider (RHIC) and the LHC [26,27]. The extension of HYDJET++ to the triangular flow was done in Ref. [28]. The interplay of v_2 and v_3 in the model describes the nonlinear contributions of elliptic and triangular flow to higher flow harmonics including the hexagonal one [28,29], as well as the long-range dihadron correlations, known as ridge [30]. Triangular flow is a very important ingredient of the model and it is thus worth discussing the features of its generation.

Anisotropic flow emerges in HYDJET++ because of the following reasons. The profile of the nuclear overlap zone in the transverse plane can be approximated by an ellipse with the spatial eccentricity $\varepsilon(b) = (R_y^2 - R_x^2)/(R_y^2 + R_x^2)$, where b is the impact parameter, and R_y and R_x are the long- and short-ellipse radii, respectively. Then, the transverse radius of the fireball reads

$$R_{\rm ell}(b,\phi) = R_{\rm fo}(b)\frac{\sqrt{1-\varepsilon^2(b)}}{\sqrt{1+\varepsilon(b)\cos 2\phi}}, \tag{3}$$

where

$$R_{\rm fo}(b) \equiv \sqrt{\left(R_x^2 + R_y^2\right)/2} = R_0\sqrt{1-\varepsilon(b)}, \tag{4}$$

with R_0 being the freeze-out transverse radius in a perfectly central collision with $b = 0$. Because every fluid cell is carrying a certain momentum, the spatial anisotropy at the freeze-out will be transformed into the momentum anisotropy. Unlike several other models, HYDJET++ does not rely on isotropic parametrization, where the azimuthal angle of the fluid velocity, $\phi_{\rm fluid}$, coincides with the azimuthal angle ϕ. Instead, these two angles are correlated via the nonlinear function [20]

$$\tan\phi_{\rm fluid} = \sqrt{\frac{1-\delta(b)}{1+\delta(b)}}\tan\phi, \tag{5}$$

where the new anisotropy parameter, $\delta(b)$, is introduced. Both spatial and flow anisotropy parameters, $\varepsilon(b)$ and $\delta(b)$, are proportional to the initial spatial anisotropy $\varepsilon_0 = b/(2R_A)$. Their values are fixed after fitting the HYDJET++ calculations to the measured elliptic flow.

To extend the model to the triangular flow the transverse radius of the freeze-out hypersurface was modified accordingly [28]:

$$R_{\rm trian}(b,\phi) = R_{\rm ell}(b,\phi)\{1 + \varepsilon_3(b)\cos[3(\phi - \Psi_3)]\}. \tag{6}$$

Because experiments show no correlation between the event planes of the second and third harmonics, i.e., $v_2(\Psi_3) = v_3(\Psi_2) = 0$, these planes are also uncorrelated in HYDJET++. The new parameter $\varepsilon_3(b)$ entering Eq. (6) is responsible for the creation of triangularity in the system. Similarly to $\varepsilon(b)$, it can also be proportional to the initial eccentricity $\varepsilon_0(b)$ or considered as a free parameter.

Note, that the model possesses event-by-event (EbyE) fluctuations even when the values of the anisotropy parameters, $\varepsilon(b)$, $\delta(b)$, and $\varepsilon_3(b)$, are fixed at the fixed impact parameter b. The sources of the EbyE fluctuations are fluctuations in particle multiplicities, coordinates, and momenta, as well as production of minijets and decays of resonances. Recently, HYDJET++ was extended [31] to match the measured EbyE fluctuations quantitatively. For this purpose the three parameters were not fixed anymore but rather smeared normally around their most probable values. The smearing procedure, however, does not change the distributions of either differential $v_{2(3)}(p_T,b)$ or p_T-integrated $v_{2(3)}(b)$ characteristics, because these results are obtained after the averaging over quite substantial amounts of generated events.

III. TRIANGULAR FLOW IN Pb + Pb COLLISIONS AT LHC

The transverse momentum dependence and the centrality dependence of the triangular flow of hadrons were studied in Pb + Pb collisions at center-of-mass energy $\sqrt{s_{NN}} = 2.76$ TeV. The considered p_T interval was $0 \leqslant p_T \leqslant 8\,\mathrm{GeV}/c$, whereas the centrality range $0 \leqslant \sigma/\sigma_{\mathrm{geo}} \leqslant 50\%$ was subdivided into five bins, namely, 0–10%, 10–20%, 20–30%, 30–40%, and 40–50%. Because the yields of hadrons with transverse momenta larger than $1\,\mathrm{GeV}/c$ rapidly drop, the generated event statistics was about 1 000 000 events for each centrality bin to provide reliable values for v_3 at $p_T \geqslant 4$ GeV/c. A detailed comparison of the HYDJET++ calculations of v_3 to the corresponding data by the ATLAS Collaboration [32] and the CMS Collaboration [33] was done in Ref. [28]. In the present article our primary goal is to reveal the contributions of different processes to the formation of triangular flow. We start from the interplay of soft processes and jets.

A. Interplay of soft and hard processes

In what follows, we distinguish between the spectra of particles

(i) directly frozen at the freeze-out hypersurface in hydro calculations (direct hydro),
(ii) direct hydro + resonance decays (soft processes only),
(iii) directly produced in jet fragmentation,
(iv) directly produced from jets + resonance decays (hard processes only),
(v) directly produced from hydro and jets, and
(vi) produced in all processes, i.e., hydro + jets + resonance decays.

Figure 1 shows the $v_3(p_T)$ spectrum of charged hadrons produced in collisions with centrality $20\% \leqslant \sigma/\sigma_{\mathrm{geo}} \leqslant 30\%$.

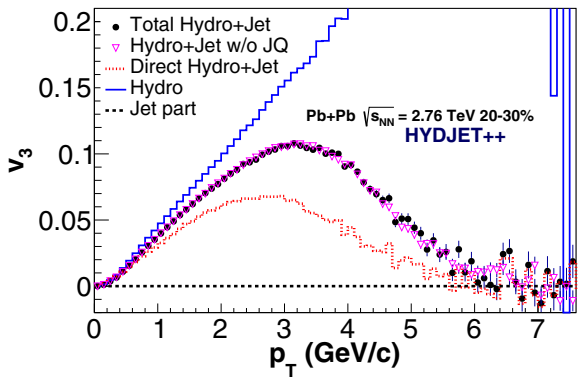

FIG. 1. The p_T dependence of different components of the triangular flow of charged particles produced in the HYDJET++ model for Pb + Pb collisions at $\sqrt{s_{NN}} = 2.76$ TeV at centrality 20–30%. The shown distributions are the $v_3(p_T)$ of particles coming from the hydro part (ii) (solid line), from the jets (iii) (dashed line), and of directly produced particles in both soft and hard (v) interactions (dotted line). Final triangular flow (vi) is presented by the solid circles, and triangles indicate the v_3 calculated without the jet quenching.

In addition to the resulting triangular flow (vi), the partial contributions coming from the hydrodynamic part with resonances (ii), the jet fragmentation (iii), and particles produced either at the freeze-out hypersurface or decoupled from jets (v) are displayed as well. To study the influence of the jet-medium interaction on the triangular flow, we plot in Fig. 1 also the calculations without the jet quenching. Note that the triangular flow of hadrons originated from the jets both with and without the jet quenching is consistent with zero in the model. Hadrons coming from soft hydrodynamic processes demonstrate an almost linear rise of triangular flow with increasing transverse momentum at $0.3 \leqslant p_T \leqslant 4$ GeV/c. Hydrodynamics, however, dominates the particle production at $p_T \lesssim 2.5$ GeV/c only, whereas at higher transverse momenta the particle spectrum is dominated by the jet hadrons. These circumstances cause the falloff of the $v_3(p_T)$ at $p_T \gtrsim 3.5$ GeV/c. The jet quenching enhances the yield of hadrons with low and intermediate transverse momenta. These particles should reduce the triangular flow in low- and intermediate-p_T ranges. However, their admixture is very small compared to hadrons produced in soft processes. As one can see in Fig. 1, the impact of the jet quenching on the development of the p_T-differential v_3 is insignificantly small. Decays of resonances increase the triangular flow of charged hadrons at $p_T \geqslant 1$ GeV/c. This follows from the comparison of $v_3(p_T)$ of hadrons directly frozen at the freeze-out hypersurface or produced in the course of the jet fragmentation (dotted curve) with the total signal (solid circles), which includes also the hadrons coming from the decays of resonances. The detailed discussion of the influence of resonance decays on the triangular flow is given in Sec. III B.

Transverse momentum distributions of the triangular flow (vi) of most abundant charged hadrons, such as pions, kaons, (anti)protons, and (anti)Λ's are depicted in Fig. 2(a) together with the hydrodynamic parts (ii) of their spectra, shown separately in Fig. 2(b). Several things are worth mentioning here. In hydrodynamic calculations both meson and baryon branches show a linear rise at $0.5 \leqslant p_T \leqslant 5$ GeV/c. Mesonic flow is stronger than that of (anti)protons, whereas for full hydro+jets calculations this is true only for $p_T \leqslant 2.5$ GeV/c. At higher transverse momenta the triangular flow of protons and antiprotons, $v_3^{\bar{p}+p}(p_T)$, continues to rise, while the triangular flow of charged pions, $v_3^{\pi^\pm}(p_T)$, and kaons, $v_3^{K^\pm}(p_T)$, drops. This effect is also caused by the jet hadrons. The heavier the particle, the harder its p_T-spectrum in hydrodynamics is. Thus, jets start to reduce the $v_3(p_T)$ distribution of heavy hadrons at larger transverse momenta compared to light hadrons, as seen in Fig. 2(a).

Recently, the triangular flow of identified hadrons in Pb + Pb collisions at $\sqrt{s} = 2.76$ TeV was measured at different centralities by the ALICE Collaboration [34]. The results of HYDJET++ calculations for charged pions, kaons, and protons with antiprotons are plotted onto the experimental data in Fig. 3 for four centrality bins, 10–20%, 20–30%, 30–40%, and 40–50%. It follows from the comparison that the model provides a fair description of the data. It reproduces correctly the mass ordering of hadron v_3 at $p_T \leqslant 2$ GeV/c and its violation at higher transverse momenta.

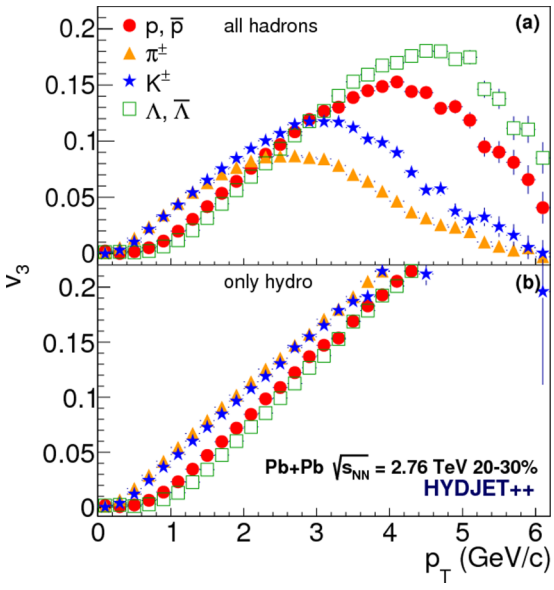

FIG. 2. The p_T dependence of (a) total triangular flow (vi) and (b) its hydro component (ii) in the HYDJET++ model for Pb + Pb collisions at $\sqrt{s_{NN}} = 2.76$ TeV at centrality 20–30%. The hadron species are $p + \bar{p}$ (solid circles), charged pions (solid triangles), charged kaons (solid stars), and $\Lambda + \overline{\Lambda}$ (open squares).

B. Influence of resonances

The differential spectra $v_3(p_T)$ of $\pi^{\pm}$, $K^{\pm}$, $p + \bar{p}$, and $\Lambda + \overline{\Lambda}$ are displayed in Fig. 4 for (semi)central (0–10%) collisions and in Fig. 5 for semiperipheral (30–40%) collisions. Here the spectra of hadrons directly produced either on the freeze-out hypersurface or in the course of jet fragmentation (v) are compared to the final distributions (vi), where decays of resonances are taken into account. For both centrality intervals the physical picture is qualitatively similar. Namely, decays of resonances do not vary significantly the triangular flow of hadronic species at transverse momenta below 1 GeV/c for pions and below 2 GeV/c for heavier particles. At higher transverse momenta the situation is changed. Hadrons coming from the resonance decays enhance the differential v_3 of all species and shift the maxima of the distributions by 0.5–1.0 GeV/c towards higher p_T. The maxima of $v_3(p_T)$ demonstrate the rise of about 25% with shifting centrality from 0–10% to 30–40% (cf. Figs. 4 and 5).

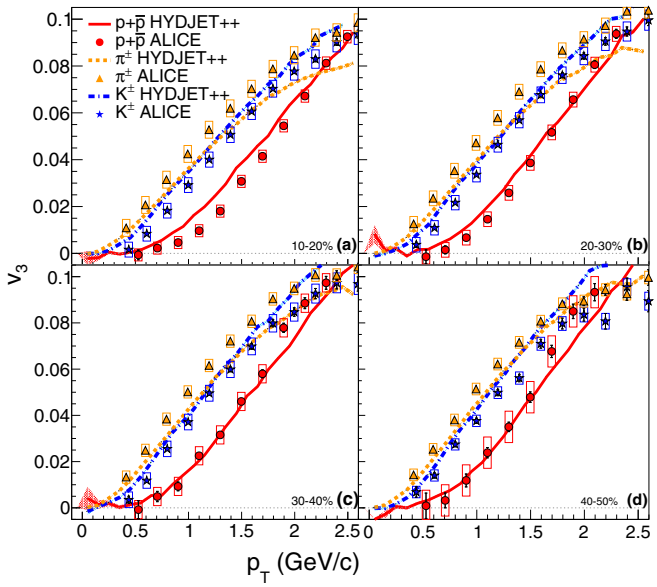

FIG. 3. The p_T dependence of triangular flow of $\pi^{\pm}$ (dashed lines), $K^{\pm}$ (dash-dotted lines), and $p + \bar{p}$ (solid lines) in HYDJET++ calculations of Pb + Pb collisions at 2.76 TeV at centrality (a) 10–20%, (b) 20–30%, (c) 30–40%, and (d) 40–50%. Corresponding experimental data from Ref. [34] are shown by solid triangles ($\pi^{\pm}$), stars ($K^{\pm}$), and circles ($p + \bar{p}$), respectively.

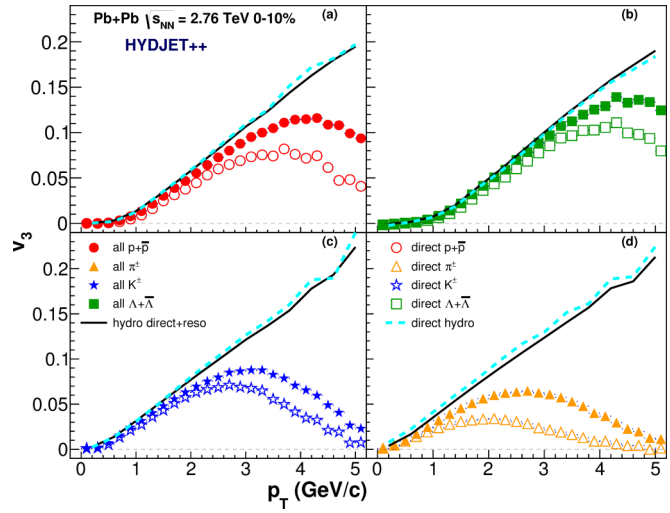

FIG. 4. The p_T dependence of triangular flow of (i) direct hadrons in hydro (dashed lines), (ii) all hadrons in hydro (solid lines), (v) direct hadrons in soft and hard processes (open symbols), and (vi) all hadrons (solid symbols) produced in the HYDJET++ model for Pb + Pb collisions at $\sqrt{s_{NN}} = 2.76$ TeV with centrality 0–10% for (a) $p + \bar{p}$, (b) $\Lambda + \overline{\Lambda}$, (c) charged kaons, and (d) charged pions.

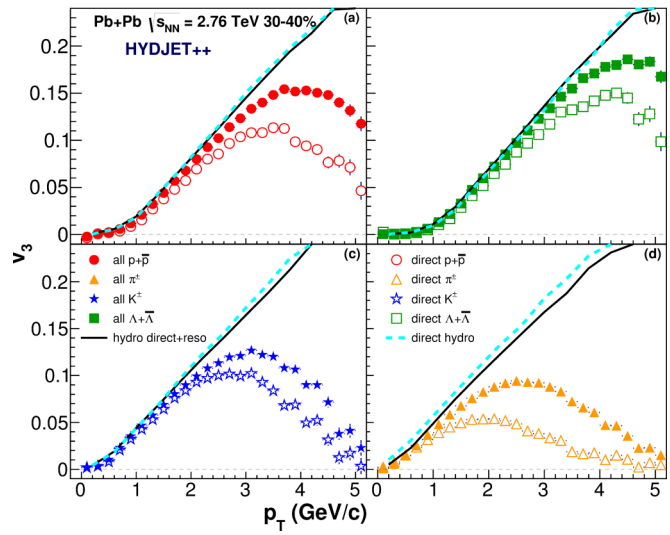

FIG. 5. The same as Fig. 4 but for centrality 30–40%.

In addition to these two distributions representing processes (v) and (vi), we plot in Figs. 4 and 5 two curves showing the $v_3(p_T)$ of particles directly produced from hydro (i) and its modification after the resonance decays (ii). For $p + \bar{p}$ and $\Lambda + \overline{\Lambda}$ both curves are very close to each other, whereas the $v_3(p_T)$ of charged kaons and, especially, of charged pions after the decays of resonances is a bit lower than that of directly produced particles. This result does not contradict the opposite behavior of the final spectra. The resonances are more abundantly produced in soft processes compared to the hard ones. Decays of resonances significantly increase the particle yields in the soft part of the spectrum; therefore fractions of hydroparticles dominate the particle spectra to larger transverse momenta. Consequently, the rise of the p_T-differential triangular flow will persist to larger values of p_T. Recall that not all resonances are equally important. As was shown in Ref. [17], the set of resonances needed for the description of the flow harmonics v_n of pions and protons can be reduced to 20–30 species only.

On the other side, the main part of particle spectrum consists of hadrons with transverse momenta lower than 1 GeV/c and pions are the dominant fraction of the spectrum, and for them the softest part of the $v_3(p_T)$ distribution seems to carry a bit weaker triangular flow after the decays of resonances compared to that of directly produced pions, as shown in Fig. 5. Therefore, the problem is twofold. First, it is necessary to scrutinize how the decays of resonances alter the pion triangular flow. After that we should get the integrated values of v_3 at different centralities.

At the energies available at the LHC of $\sqrt{s_{NN}} = 2.76$ TeV or higher only about 20% of pions are produced in HYDJET++ directly at the freeze-out hypersurface. The rest comes out as a result of decays of various resonances, both mesonic and baryonic. If we consider an isotropic decay of a baryon resonance on a pion and a lighter baryon, then, because of the decay kinematics, the daughter baryon should carry almost the same transverse momentum as the decaying resonance, whereas the pion p_T is much softer. This type of reaction will boost the triangular flow of the soft part of the pionic spectrum because the averaged triangular flow of heavy resonances is larger than that of pions. For meson resonances the softening or hardening of the pion triangular flow depends on the number of pions in the final state. To illustrate this let us consider three decays: $\rho \to \pi\pi$ (26% of pion yield), $\omega \to \pi\pi\pi$ (11%), and $\Delta \to p + p/\bar{p}$ (less than 2%). The differential $v_3(p_T)$ of these resonances and their decay products are compared in Fig. 6 to the triangular flow of directly produced pions and (anti)protons. The triangular flow of pions from ρ decays is just a bit softer than the v_3 of ρ mesons. Consequently, it is harder than the triangular flow of direct pions at $p_T \leqslant 1.5$ GeV/c [see Fig. 6(a)]. The spectrum of pions from ω decays, in contrast, is much softer than that of ω's. Thus, their triangular flow at $p_T \leqslant 1.5$ GeV/c is even stronger than that of the direct pions. A similar tendency is revealed by pions from the Δ decays. Therefore, some resonances will enhance the pion triangular flow in the soft p_T region, whereas other will reduce it.

The result of this interplay is seen in Fig. 7, which shows the integrated values of the triangular flow of charged hadrons calculated in five centrality bins. The triangular flow of direct particles and that of direct particles together with products of resonance decays obtained in the hydro part of the model are shown separately. To compare the model results to the experimental data, the integration over the transverse momentum was done in two intervals: $1 \leqslant p_T \leqslant 2$ GeV/c, displayed in Fig. 7(a), and $2 < p_T \leqslant 3$ GeV/c, displayed in Fig. 7(b). Experimental data from the ATLAS Collaboration [32] are plotted onto the HYDJET++ calculations. We see that decays of resonances just slightly reduce the integrated v_3. The triangular flow at $2 < p_T \leqslant 3$ GeV/c in the hydrodynamic part is almost twice as strong as the v_3 at $1 \leqslant p_T \leqslant 2$ GeV/c. Jets significantly diminish the triangular flow in both p_T intervals.

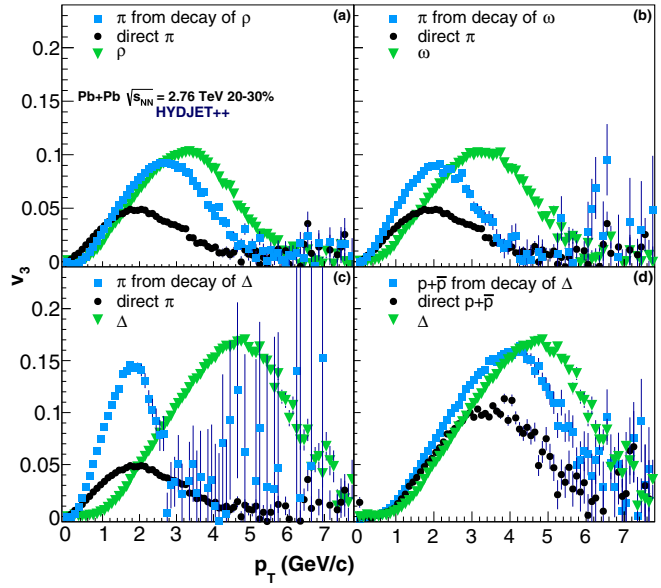

FIG. 6. The p_T dependence of triangular flow of charged pions produced both directly (circles) and in decays (squares) of (a) ρ and (b) ω, respectively, in the HYDJET++ model for Pb + Pb collisions at $\sqrt{s_{NN}} = 2.76$ TeV with centrality 20–30%. (c) and (d) The same as panels (a) and (b) but for (c) charged pions and (d) $p + \bar{p}$ produced in decays of Δ's. The flow of resonances is shown in each window by triangles.

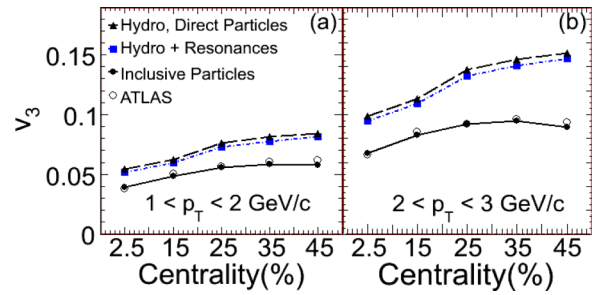

FIG. 7. p_T-integrated triangular flow of inclusive charged hadrons with (a) $1 \leqslant p_T \leqslant 2$ GeV/c and (b) $2 < p_T \leqslant 3$ GeV/c as a function of centrality in Pb + Pb collisions at $\sqrt{s_{NN}} = 2.76$ TeV. Triangles and squares present the calculations for direct particles (i) and direct plus decays of resonances (ii), respectively, only in the hydro part of the model. Final results are shown by solid circles, and open circles are the experimental data from Ref. [32]. Lines are drawn to guide the eye.

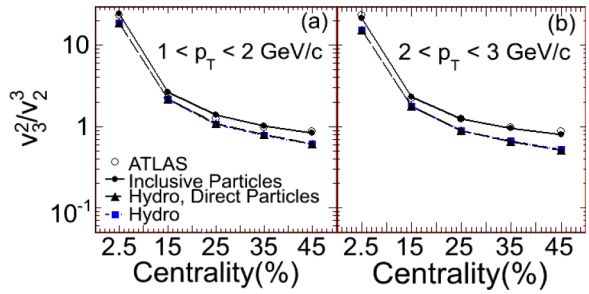

FIG. 8. The same as Fig. 7 but for the ratio v_3^2/v_2^3 of p_T-integrated triangular and elliptic flow.

C. Ratio $v_3^{1/3}/v_2^{1/2}$

The ratios $v_n^{1/n}/v_2^{1/2}$ were suggested in Ref. [32] as a probe to study the possible scaling properties of the flow harmonics. The ratio of triangular and elliptic flow, where both harmonics are integrated over the transverse momentum range, reveals no indication of the scaling trend. The results are presented in Fig. 8. As in the previous figure, two groups of hadrons are selected, one with $1 \leqslant p_T \leqslant 2$ GeV/c and another with $2 < pT \leqslant 3$ GeV/c to compare the HYDJET++ calculations to the experimental data. To see the changing of the ratio with increasing impact parameter more distinctly, the ratio v_3^2/v_2^3 is used. Again, the decays of resonances make no impact on the ratio, which clearly drops as the reaction becomes more peripheral. Note that jets increase the final ratio compared to the pure hydro part. We should come back to this point later.

If the ratio $v_3^{1/3}/v_2^{1/2}$ is plotted as a function of transverse momentum in various centrality bins, as shown in Fig. 9, then the considered distributions are remarkably flat. The ratios $v_3^{1/3}(p_T)/v_2^{1/2}(p_T)$ do not depend on p_T in a quite broad range of transverse momentum from 1 GeV/c up to 6 GeV/c. This p_T independence, however, is not predefined in HYDJET++,

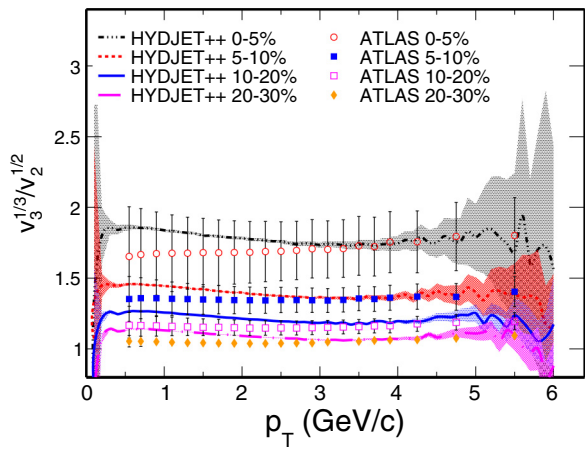

FIG. 9. Ratio $v_3^{1/3}/v_2^{1/2}$ as a function of p_T in centrality bins 0-5% (dotted line), 5–10% (dashed line), 10–20% (solid line), and 20–30% (dash-dotted line). Shaded areas indicate the statistical error bands in the model. The corresponding ATLAS data from Ref. [32] are shown by open circles, filled squares, open squares, and diamonds, respectively.

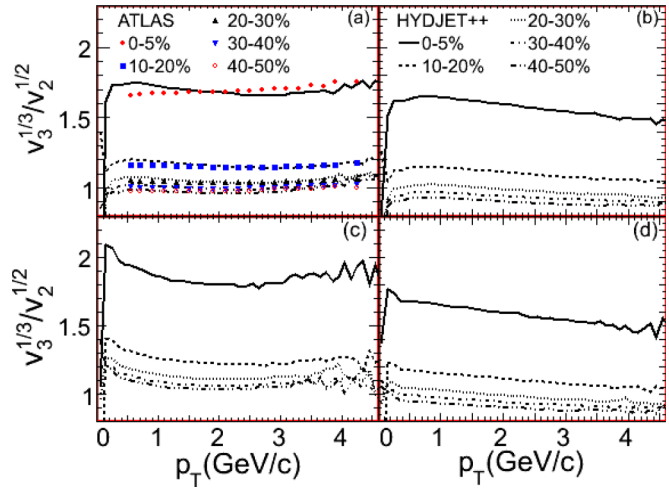

FIG. 10. The same as Fig. 9 but for (a) ratios of total signals in 0–5% (solid curve), 10–20% (dashed curve), 20–30% (dotted curve), 30–40% (dash-dotted curve), and 40–50% (dash-dot-dotted curve) centrality bins; (b) ratios of only hydrodynamic parts (ii) of both flows; (c) ratios of the flow harmonics for only directly produced particles (v); and (d) ratios of the flow harmonics for only directly produced particles in the hydrodynamic part of the model (i).

but arises as a result of nontrivial interplay between soft and hard processes.

To study this effect we selected from the particle spectrum the following types of hadrons: directly produced hadrons (v), hadrons directly produced in the soft processes only (i), and hadrons from direct hydro plus the hadrons from resonance decays (ii). The calculated ratios $v_3^{1/3}(p_T)/v_2^{1/2}(p_T)$ are depicted in Fig. 10. In Fig. 10(d) one can see that this ratio decreases with rising p_T for directly produced hadrons in the hydromodulus of the model for all centrality intervals. Decays of resonances make the slopes of the ratios less steep [see Fig. 10(b)]. Finally, the rise of the tails at $p_T \geqslant 2$ GeV/c is provided by the jet particles, as shown in Fig. 10(c). Here the jets and the final-state interactions are working together towards the formation of a plateau at $1 \leqslant p_T \leqslant 6$ GeV/c. At higher transverse momenta jets may cause the rise of the ratio, similar to that of $v^{1/4}/v_2^{1/2}$, observed both experimentally [35] and in HYDJET++ [27]. The lack of statistics and large error bars, however, does not permit us to make more definite conclusions.

D. NCQ scaling

The NCQ scaling was first observed for the elliptic flow of hadron species in Au + Au collisions at the energy available at the RHIC of $\sqrt{s_{NN}} = 200$ GeV [36,37]. It was found that if one plots the v_2 as a function of the transverse kinetic energy of the hadron, $KE_T \equiv m_T - m_0$, and divides both v_2 and KE_T by the number of constituent quarks in the hadron, n_q, then the excitation functions $v_2^{\text{hadr}}(KE_T/n_q)/n_q$ of different hadrons sit on the top of each other up to $KE_T/n_q \approx 0.8$–1.0 GeV [38]. It was pointed out in Refs. [24,25] that, because of the stronger jet influence, the fulfillment of the NCQ scaling at the LHC should be worsened compared to that at the RHIC. The worsening of

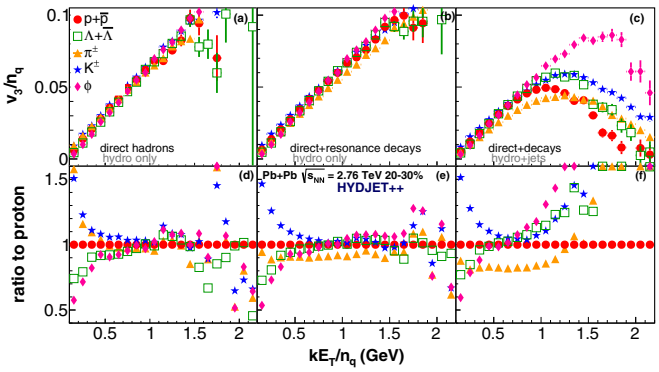

FIG. 11. Upper row: The KE_T/n_q dependence of the triangular flow for (a) direct hadrons (i), (b) hadrons produced in soft processes only (ii), and (c) hadrons produced both in soft and hard processes (vi) in the HYDJET++ model in Pb + Pb collisions at $\sqrt{s_{NN}} = 2.76$ TeV with centrality 20–30%. The considered hadron species are: $p + \bar{p}$ (solid circles), $\Lambda + \overline{\Lambda}$ (open squares), $\pi^{\pm}$ (solid triangles), $K^{\pm}$ (stars), and ϕ (diamonds). Bottom row: The KE_T/n_q dependence of the distributions in the upper row normalized to the triangular flow of $p + \bar{p}$, $(v_3/n_q)/(v_3^{p+\bar{p}}/3)$.

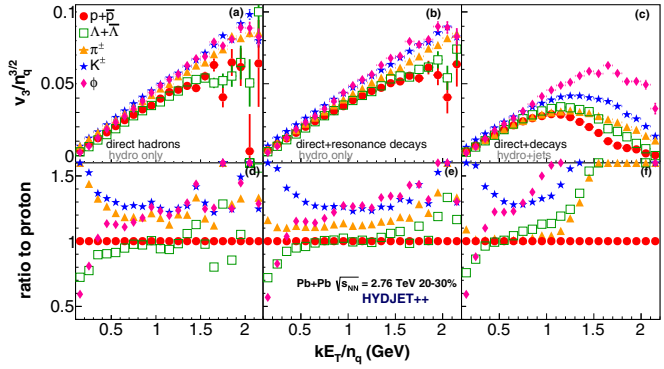

FIG. 12. The same as Fig. 11 but for $v_3(KE_T/n_q)/n_q^{3/2}$ distributions.

the NCQ scaling conditions for the elliptic flow at the LHC was later observed by the ALICE Collaboration [39,40].

It is instructive, therefore, to check the NCQ scaling for the triangular flow of hadronic species at $\sqrt{s_{NN}} = 2.76$ TeV. To elaborate on the role of final-state interactions and the hard processes, we plot in Fig. 11 separately (a) the triangular flow of the main hadron species produced directly on the freeze-out hypersurface (i), (b) then added to their spectra the flow of particles produced after the decays of resonances (ii), and finally (c) the resulting v_3 of hadrons produced in both soft and hard processes (vi). For clarity, all distribution functions $v_3^{\rm hadr}(KE_T/n_q)/n_q$ were also normalized to that of (anti)protons, shown in the bottom row of Fig. 11. One can see in Fig. 11(a) that the NCQ scaling is fulfilled in HYDJET++ within the 10% accuracy limit for the v_3 of main hadron species, frozen already at the freeze-out hypersurface, in the range $0.5 \leqslant KE_T \leqslant 1.2$ GeV. This occurs because, as we already saw in Figs. 4 and 5, resonances increase the triangular flow of lighter hadrons at intermediate p_T and shift the maxima of their differential distributions to higher p_T values. Some hadrons, such as ϕ mesons, do not get the feed-down from resonances, thus their distributions become closer to those of light mesons at intermediate transverse momenta. However, at $p_T \gtrsim 3$ GeV/c the particle spectra are dominated by the jet hadrons, for which the scaling conditions are not relevant. The hadrons fragmenting from jets lead to only approximate fulfillment of the NCQ scaling for the hadron triangular flow in the interval $0.15 \leqslant KE_T \leqslant 1.1$ GeV.

It was suggested in Ref. [41] to use the ratio $v_n^{\rm hadr}/(n_q)^{n/2}$ instead of the standard $v_n^{\rm hadr}/n_q$ to search for the NCQ scaling of the nth flow harmonic. The modified scaling for 0–50% central Au + Au collisions at the highest energy available at the RHIC was observed for v_2, v_3, and v_4 [42]. The HYDJET++ distributions $v_3^{\rm hadr}/n_q^{3/2}$ are shown in Fig. 12. Only approximate scaling within ±15% margins is seen for hadrons with $0.5 \leqslant KE_T \leqslant 1.5$ GeV produced in soft processes. When jets are taken into account, the interval of approximate scaling fulfillment for all but ϕ mesons shrinks to $0.5 \leqslant KE_T \leqslant 1.0$ GeV.

IV. CONCLUSIONS

The triangular flow v_3 of charged inclusive and identified hadrons was studied within the HYDJET++ model in Pb + Pb collisions at $\sqrt{s_{NN}} = 2.76$ TeV and centralities $0\% \leqslant \sigma/\sigma_{\rm geo} \leqslant 50\%$. The model couples soft hydrolike states to hard processes and contains an extended table of resonances, thus allowing for investigation of the interplay between soft processes, jets, and resonance decays on the formation of particle v_3. The results can be summarized as follows.

The triangular flows of identified hadrons produced in soft processes display an almost linear rise at $0.3 \leqslant p_T \leqslant 5$ GeV/c. The mass ordering effect is achieved, i.e., the flow of mesons is stronger than that of baryons. The fraction of hadrons produced in jet fragmentation is the most abundant in particle spectra at $p_T \geqslant 2.5$ GeV/c. Since these hadrons carry almost no v_3, the distribution functions $v_3(p_T)$ experience a falloff at intermediate transverse momenta. The interplay of hard and soft processes leads also to breaking of the mass ordering of the triangular flow, because jet particles start to dominate spectra of heavy hadrons at larger p_T compared to those of light hadrons. It appears that switching off the jet quenching does not influence the final differential triangular flow $v_3(p_T)$. Model calculations agree well with recent experimental data.

Decays of resonances distinctly modify the differential distributions of hadrons $v_3(p_T)$ at $p_T \geqslant 2$ GeV/c. The maxima of the spectra become about 25% higher. Simultaneously, they are shifted by 0.5–1.0 GeV/c towards higher transverse momenta. In contrast, the influence of resonance decays on the p_T-integrated triangular flow is extremely small.

The flatness of the ratios $v_3^{1/3}(p_T)/v_2^{1/2}(p_T)$ at different centralities emerges in HYDJET++ as a result of interplay of final-state interactions and jets. These ratios decrease with rising transverse momenta for particles directly frozen at the freeze-out hypersurface. Decays of resonances reduce the

values of $v_3^{1/3}/v_2^{1/2}$ at low p_T, whereas the jet hadrons boost their high-p_T tails, thus leading to independence of the ratios on transverse momentum in a broad range of $0.5 \leqslant p_T \leqslant 5$ GeV/c.

The two mechanisms, however, work in opposite directions when we consider the fulfillment of the NCQ scaling for the triangular flow. In this case decays of resonances enhance the high-p_T parts of the $v_3^{\rm hadr}(KE_T/n_q)/n_q$ spectra of light hadrons, thus extending the upper KE_T limit of the NCQ scaling performance. Jet particles, in their turn, carry very weak flow and wash out the signal. We verified also the NCQ scaling conditions for $v_3^{\rm hadr}(KE_T/n_q)/n_q^{3/2}$ distributions. The result stays put; i.e., hadrons decoupling from jets are worsening the scaling, while the final-state interactions act toward its fulfillment.

ACKNOWLEDGMENTS

Fruitful discussions with M. Bleicher, L. Csernai, I. Mishustin, and H. Stöcker are gratefully acknowledged. We thank also our colleagues from the CMS, ALICE, and ATLAS Collaborations for the extended cooperation. This work was supported in part by Grant No. INGO II LG15001 of the Ministry of Education, Youth and Sports of the Czech Republic; the Grant Agency of Czech Republic under Grant No. 13-20841S; the Department of Physics, University of Oslo; the Frankfurt Institute for Advanced Studies (FIAS); and a grant from the President of Russian Federation for Scientific Schools (Grant No. 7989.2016.2). L.B. acknowledges the financial support of the Alexander von Humboldt Foundation. B.H.B.J. acknowledges the financial support of the Norwegian Research Council (NFR).

[1] H. Stöcker and W. Greiner, Phys. Rep. **137**, 277 (1986).
[2] W. Reisdorf and H. G. Ritter, Annu. Rev. Nucl. Part. Sci. **47**, 663 (1997).
[3] L. V. Bravina, L. P. Csernai, P. Levai, and D. Strottman, Phys. Rev. C **50**, 2161 (1994).
[4] S. Voloshin and Y. Zhang, Z. Phys. C **70**, 665 (1996).
[5] A. M. Poskanzer and S. A. Voloshin, Phys. Rev. C **58**, 1671 (1998).
[6] L. P. Csernai and H. Stöcker, J. Phys. G **41**, 124001 (2014).
[7] S. A. Voloshin, A. M. Poskanzer, and R. Snellings, in *Relativistic Heavy Ion Physics*, Landolt-Börnstein Database Vol. 23, edited by R. Stock (Springer, Berlin, 2010), pp. 5–54.
[8] U. Heinz and R. Snellings, Annu. Rev. Nucl. Part. Sci. **63**, 123 (2013).
[9] B. Alver and G. Roland, Phys. Rev. C **81**, 054905 (2010).
[10] J. Velkovska *et al.* (CMS Collaboration), J. Phys. G **38**, 124011 (2011).
[11] J. Jia *et al.* (ATLAS Collaboration), J. Phys. G **38**, 124012 (2011).
[12] R. Snellings *et al.* (ALICE Collaboration), J. Phys. G **38**, 124013 (2011).
[13] H. Petersen, G.-Y. Qin, S. A. Bass, and B. Müller, Phys. Rev. C **82**, 041901 (2010).
[14] Z. Qiu and U. Heinz, Phys. Rev. C **84**, 024911 (2011).
[15] B. H. Alver, C. Gombeaud, M. Luzum, and J.-Y. Ollitrault, Phys. Rev. C **82**, 034913 (2010).
[16] M. Schulc and B. Tomášik, Phys. Rev. C **90**, 064910 (2014); J. Phys. G: Nucl. Part. Phys. **43**, 125106 (2016).
[17] Z. Qiu, C. Shen, and U. Heinz, Phys. Rev. C **86**, 064906 (2012).
[18] I. P. Lokhtin, L. V. Malinina, S. V. Petrushanko, A. M. Snigirev, I. Arsene, and K. Tywoniuk, Comput. Phys. Commun. **180**, 779 (2009).
[19] N. S. Amelin, R. Lednicky, T. A. Pocheptsov, I. P. Lokhtin, L. V. Malinina, A. M. Snigirev, Iu. A. Karpenko, and Yu. M. Sinyukov, Phys. Rev. C **74**, 064901 (2006).
[20] N. S. Amelin, R. Lednicky, I. P. Lokhtin, L. V. Malinina, A. M. Snigirev, Iu. A. Karpenko, Yu. M. Sinyukov, I. Arsene, and L. Bravina, Phys. Rev. C **77**, 014903 (2008).
[21] M. Chojnacki, A. Kisiel, W. Florkowski, and W. Broniowski, Comput. Phys. Commun. **183**, 746 (2012).
[22] I. P. Lokhtin and A. M. Snigirev, Eur. Phys. J. C **45**, 211 (2006).
[23] I. P. Lokhtin, A. V. Belyaev, L. V. Malinina, S. V. Petrushanko, E. R. Rogochaya, and A. M. Snigirev, Eur. Phys. J. C **72**, 2045 (2012).
[24] G. Eyyubova, L. V. Bravina, E. E. Zabrodin, V. L. Korotkikh, I. P. Lokhtin, L. V. Malinina, S. V. Petrushanko, and A. M. Snigirev, Phys. Rev. C **80**, 064907 (2009).
[25] E. Zabrodin, G. Eyyubova, L. Bravina, I. P. Lokhtin, L. V. Malinina, S. V. Petrushanko, and A. M. Snigirev, J. Phys. G **37**, 094060 (2010).
[26] E. Zabrodin, G. Eyyubova, L. Malinina, and L. Bravina, Acta Phys. Pol. B Proc. Suppl. **5**, 349 (2012).
[27] L. Bravina, B. H. Brusheim Johansson, G. Eyyubova, and E. Zabrodin, Phys. Rev. C **87**, 034901 (2013).
[28] L. V. Bravina, B. H. Brusheim Johansson, G. Kh. Eyyubova, V. L. Korotkikh, I. P. Lokhtin, L. V. Malinina, S. V. Petrushanko, A. M. Snigirev, and E. E. Zabrodin, Eur. Phys. J. C **74**, 2807 (2014).
[29] L. Bravina, B. H. Brusheim Johansson, E. E. Zabrodin, G. Eyyubova, V. L. Korotkikh, I. P. Lokhtin, L. V. Malinina, S. V. Petrushanko, and A. M. Snigirev, Phys. Rev. C **89**, 024909 (2014).
[30] G. Eyyubova, V. L. Korotkikh, I. P. Lokhtin, S. V. Petrushanko, A. M. Snigirev, L. Bravina, and E. E. Zabrodin, Phys. Rev. C **91**, 064907 (2015).
[31] L. V. Bravina, E. S. Fotina, V. L. Korotkikh, I. P. Lokhtin, L. V. Malinina, E. N. Nazarova, S. V. Petrushanko, A. M. Snigirev, and E. E. Zabrodin, Eur. Phys. J. C **75**, 588 (2015).
[32] G. Aad *et al.* (ATLAS Collaboration), Phys. Rev. C **86**, 014907 (2012).
[33] S. Chatrchyan *et al.* (CMS Collaboration), Phys. Rev. C **87**, 014902 (2013).
[34] J. Adam *et al.* (ALICE Collaboration), J. High Energy Phys. 09 (2016) 164.
[35] B. Abelev *et al.* (ALICE Collaboration), Phys. Lett. B **719**, 18 (2013).
[36] J. Adams *et al.* (STAR Collaboration), Phys. Rev. Lett. **92**, 052302 (2004).

[37] S. S. Adler *et al.* (PHENIX Collaboration), Phys. Rev. Lett. **91**, 182301 (2003).
[38] A. Adare *et al.* (PHENIX Collaboration), Phys. Rev. Lett. **98**, 162301 (2007).
[39] M. Krzewicki *et al.* (ALICE Collaboration), J. Phys. G **38**, 124047 (2011).
[40] F. Noferini *et al.* (ALICE Collaboration), Nucl. Phys. A **904-905**, 483c (2013).
[41] R. Lacey *et al.* (PHENIX Collaboration), J. Phys. G **38**, 124048 (2011).
[42] A. Adare *et al.* (PHENIX Collaboration), Phys. Rev. C **93**, 051902(R) (2016).